Electronic Supplementary Material (ESI) for Journal of Materials Chemistry A.

Electronic Supplementary Information

Assembled Caseins as Crosslinkers for Tough, Adhesive and Self-Healing Hydrogels towards Flexible Sensor

Xiao-Xia Li[a], Min Wang[a], Jing Dai[b], Huanhuan Liu*[a], Haili Qin*[b]

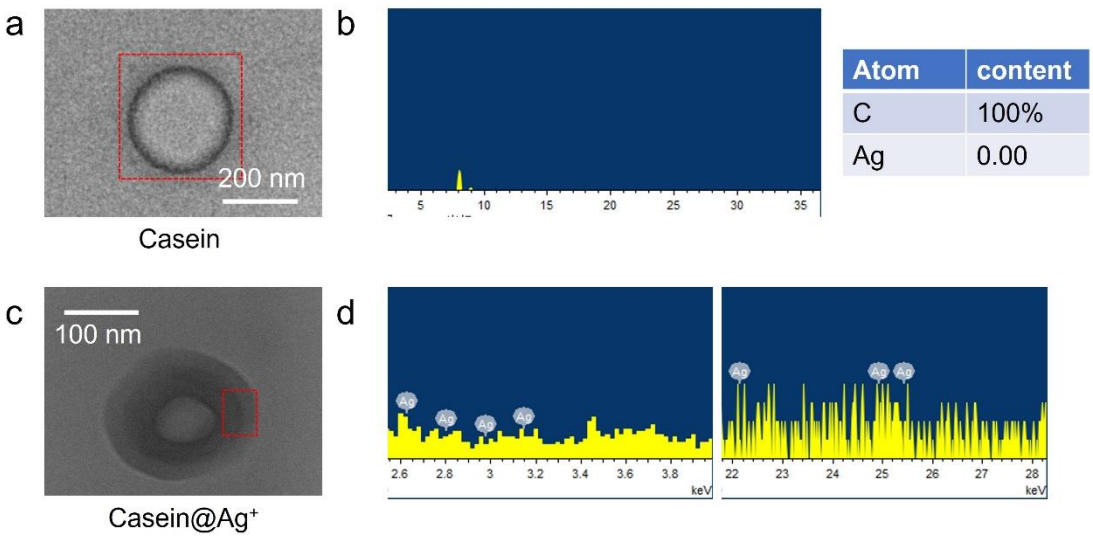

Figure S1. TEM image and EDS analysis of **(a, b)** Casein and **(c, d)**Casein@Ag^{+}.

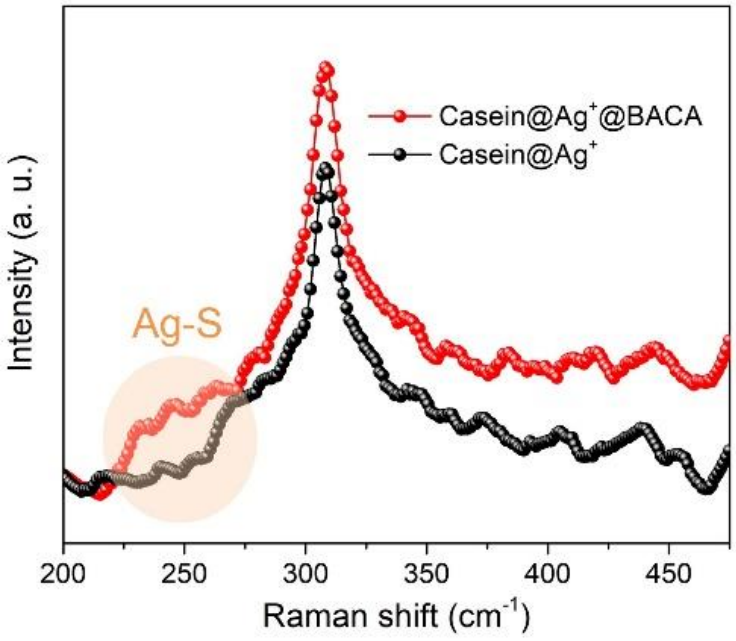

Figure S2. Raman spectra of Casein@Ag^{+}@BACA and Casein@Ag^{+}.

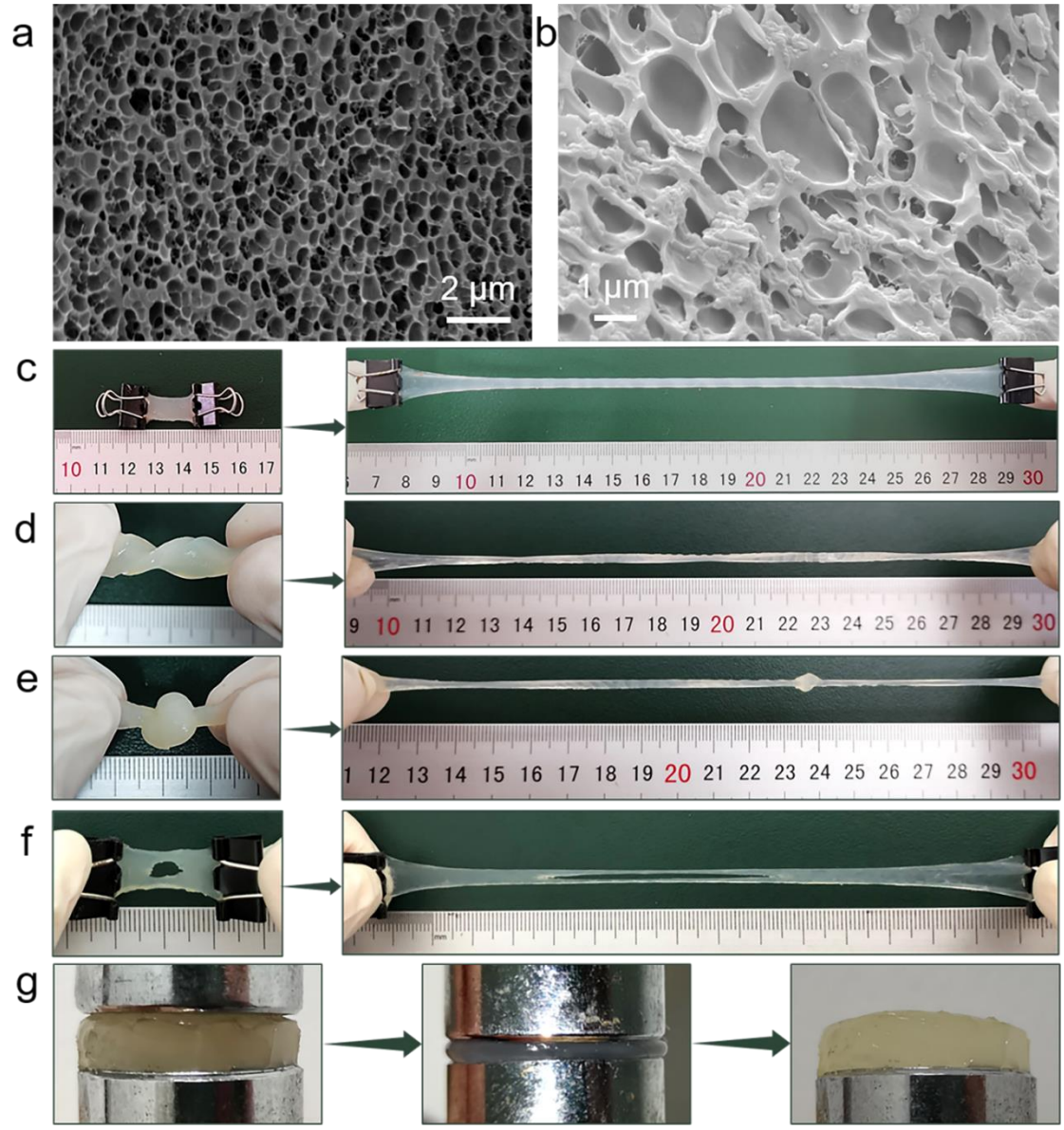

Figure S3. SEM images of freeze-dried **(a)** CAP and **(b)** CP hydrogels. **(c)** Optical images show the high stretchability of the CAP hydrogel. **(d-f)** Optical images show the CAP hydrogel with different types of deformations, such as twisting, knotting, punching, and extensive stretching. **(g)** Optical images show the excellent elastic performance to resist a high compression.

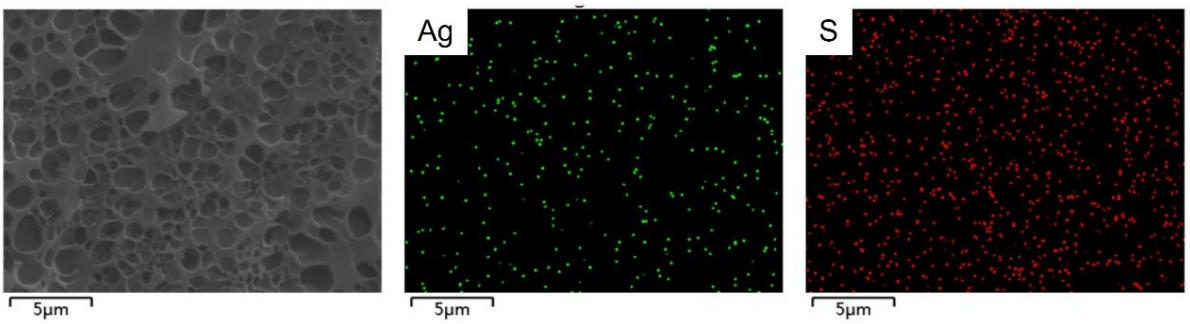

Figure S4. Element mappings of the freeze-dried CAP hydrogel showing the uniform dispersion of Ag and S.

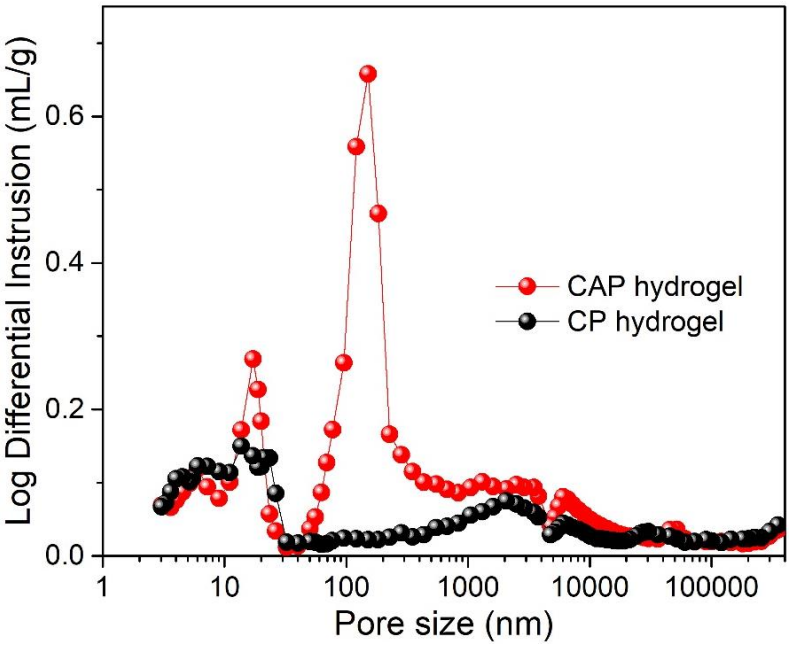

Figure S5. Detailed analysis of network structure for hydrogels using a mercury intrusion porosimeter.

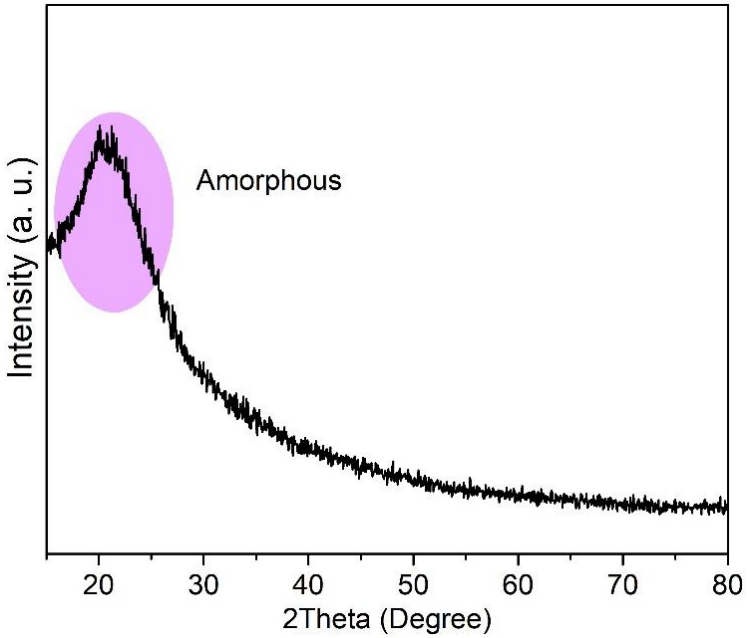

Figure S6. XRD pattern of CAP hydrogel. The broad peak at about 21° confirmed the amorphous nature of CAP hydrogel.

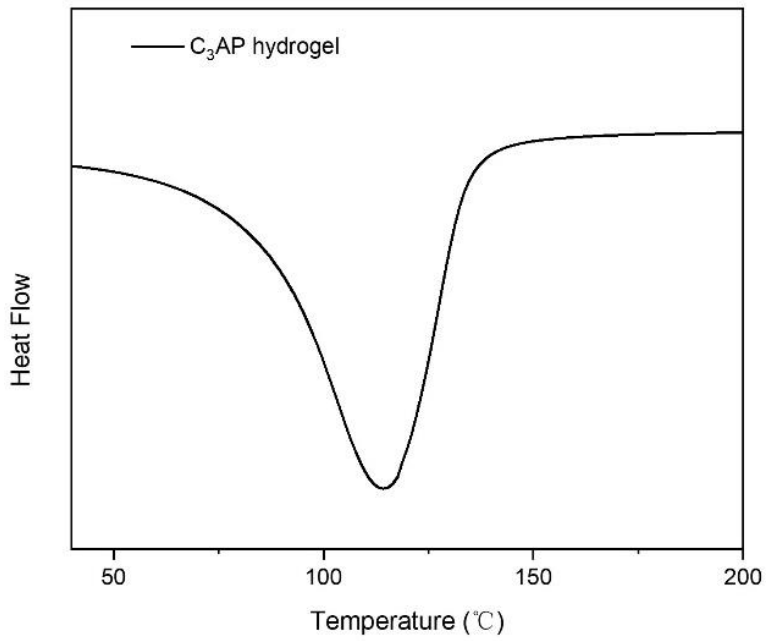

Figure S7. DSC thermogram of C_3AP hydrogel.

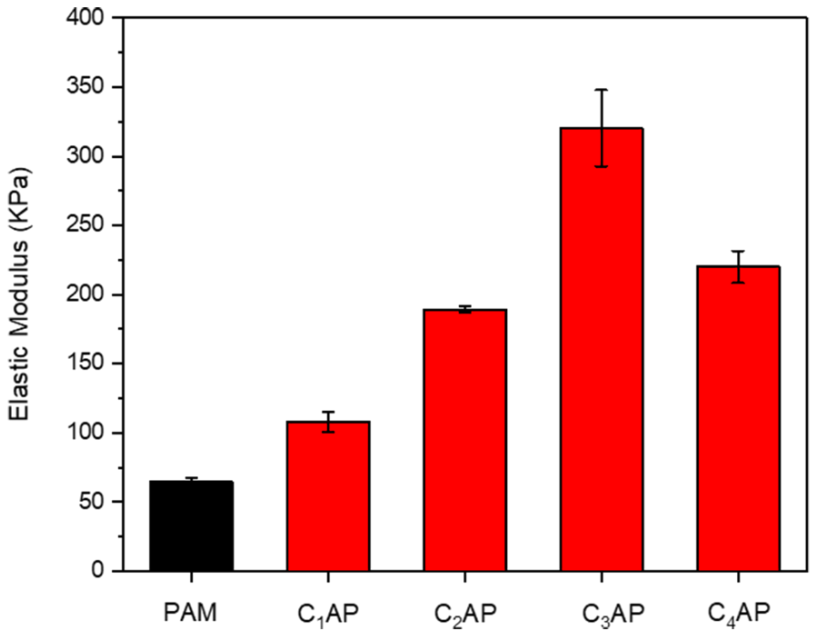

Figure S8. The tangle elastic modulus was calculated from the stress-strain curves of the PAM and CAP hydrogels as a function of casein concentration.

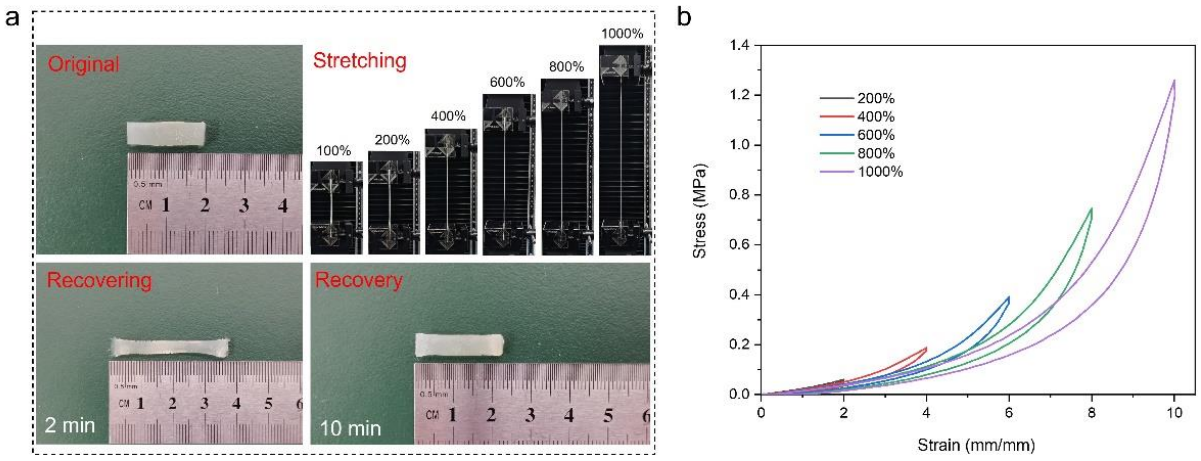

Figure S9. Self-recovery performance. **(a)** Optical images showing the stretching and self-recovering process of C_3AP hydrogel. **(b)** Tensile stress-strain curves of C_3AP hydrogel subjected to loading and unloading to measure hysteresis.

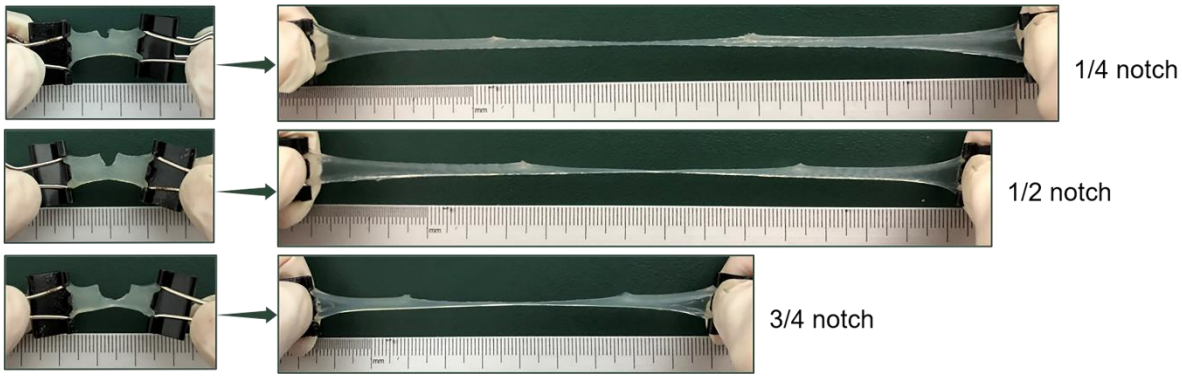

Figure S10. Optical images show the C_3AP hydrogel pieces with notches from 1/4 to 3/4 of their original widths stretched to form large deformations without rupturing.

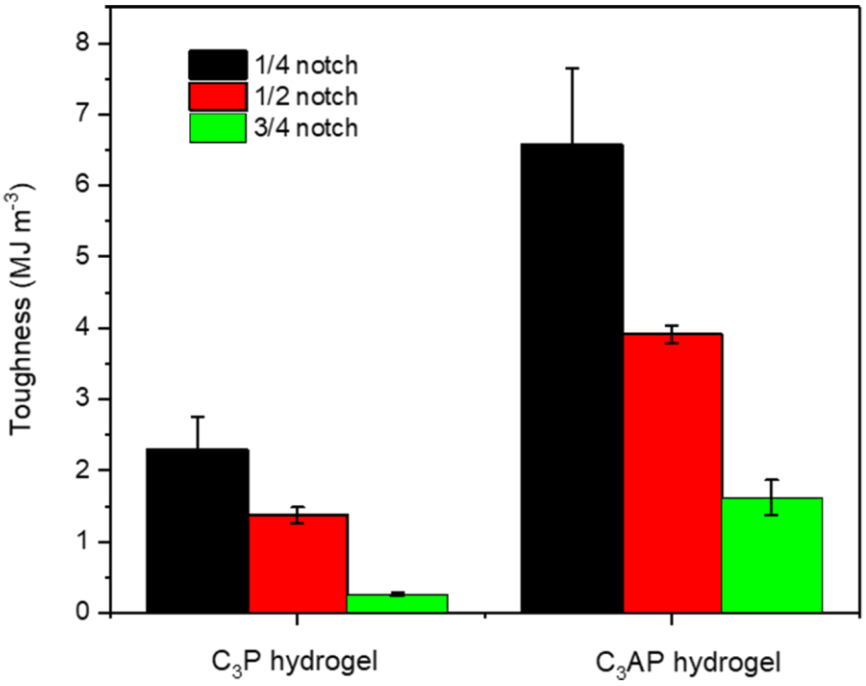

Figure S11. Histogram shows the toughness of the pristine C_3P, C_3AP hydrogels and corresponding samples with different notch proportions.

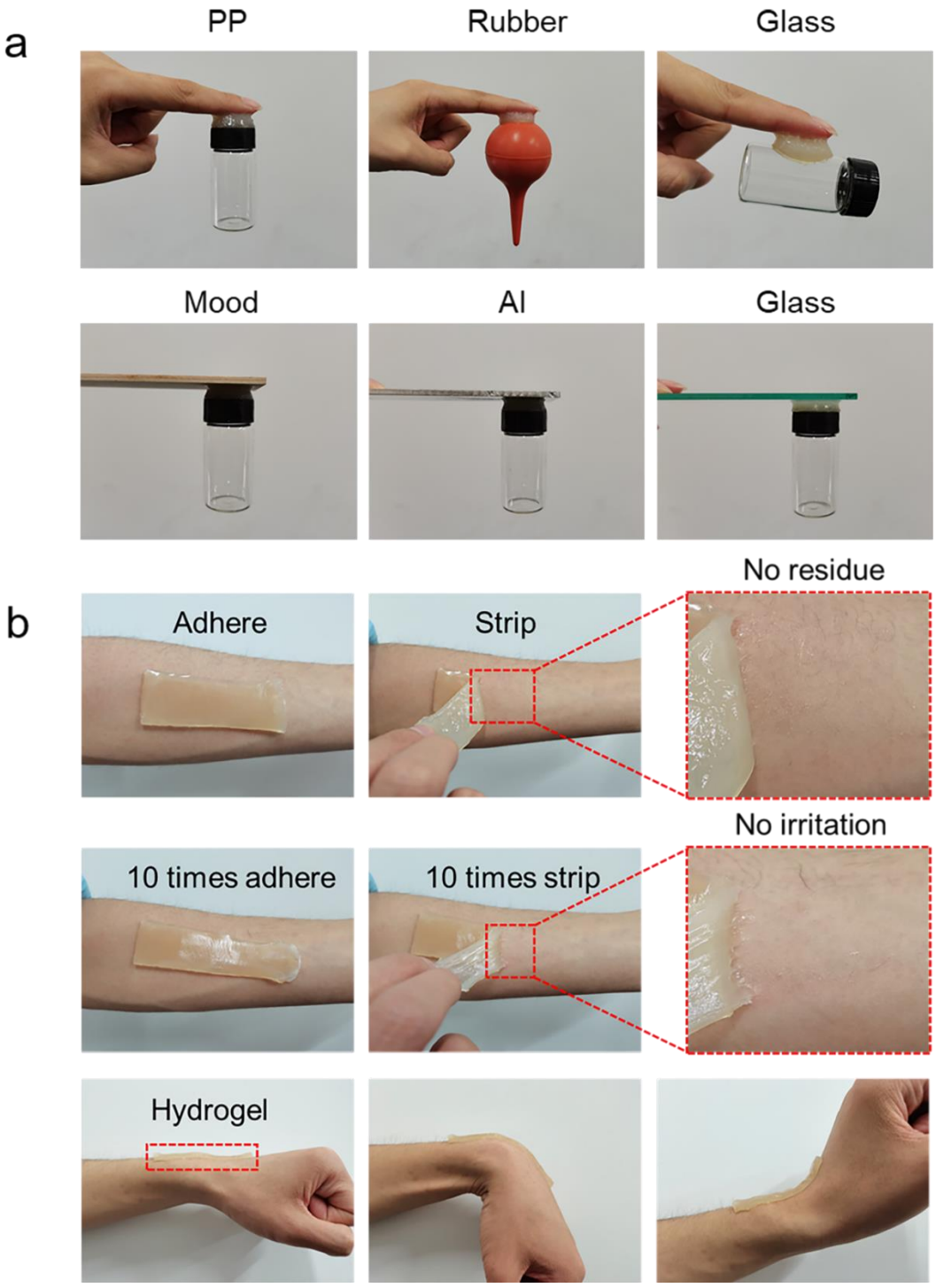

Figure S12. (a) The C_3AP hydrogel adhered to various materials. **(b)** The C_3AP hydrogel was repeatedly adhered to the skin of the author. After peeling off, no residue or irritation on the skin was found. Adhering to the elbow joint without limiting movement.

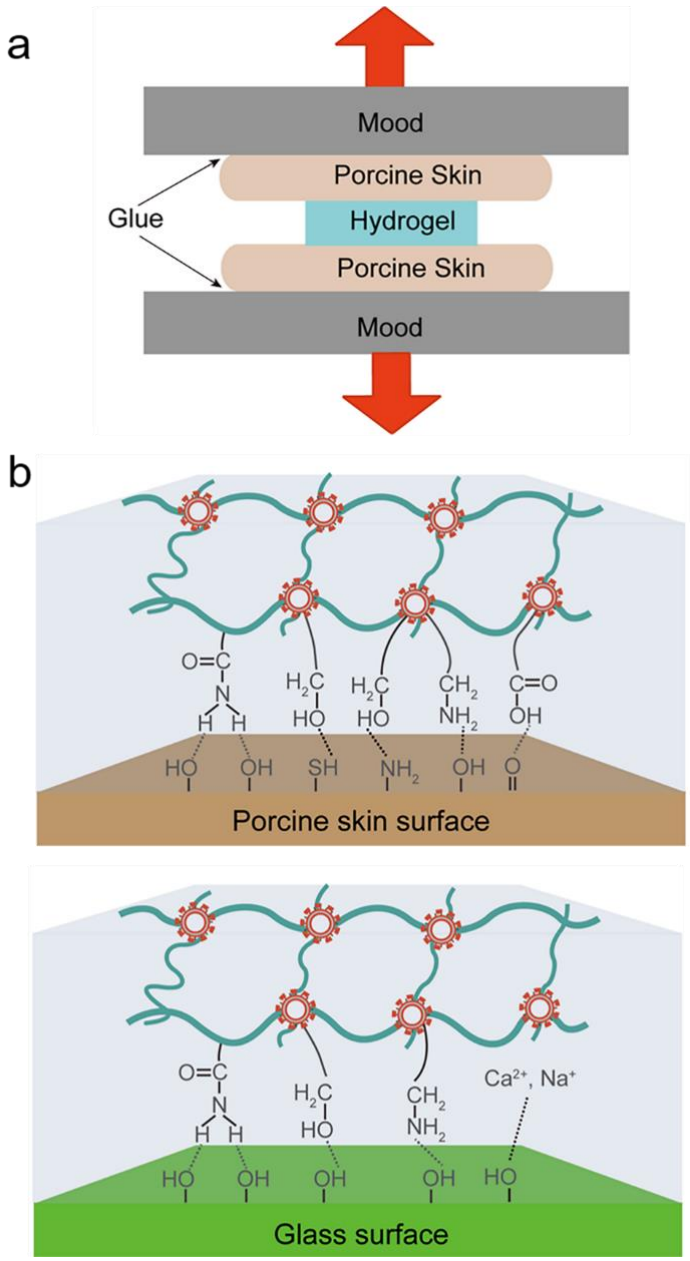

Figure S13. (a) Schematic graph of tensile-adhesion test of adhesive hydrogel on porcine skin tissue. **(b)** The adhesion mechanism of the CAP hydrogel.

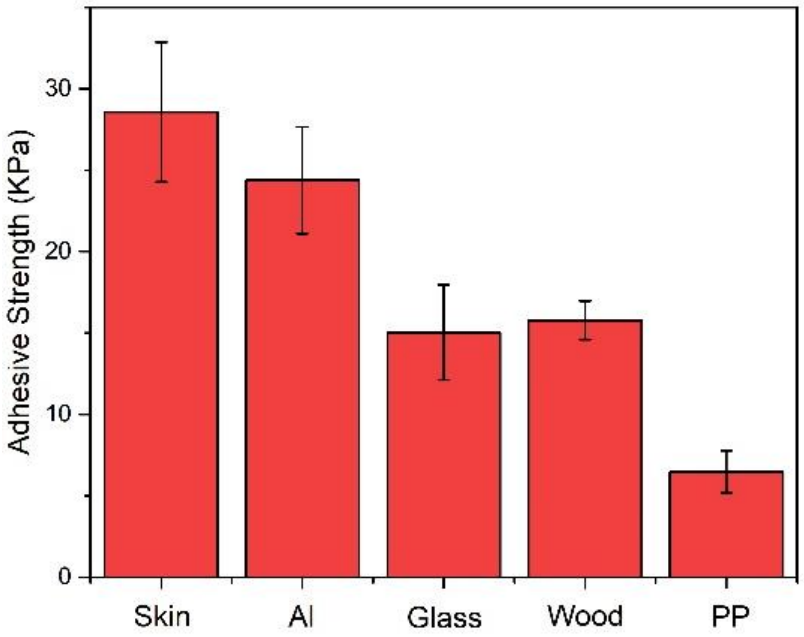

Figure S14. Adhesion strength of the C_3AP hydrogel to different substrates. Error bars showing the SD with sample size of 6.

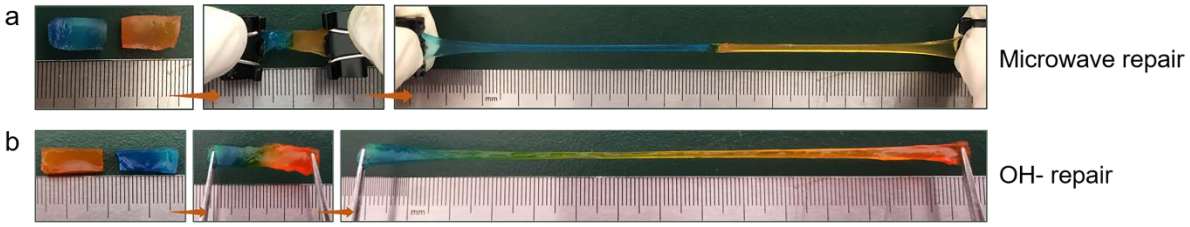

Figure S15. Optical images show the excellent healing ability of C_3AP hydrogel under different stimuli.

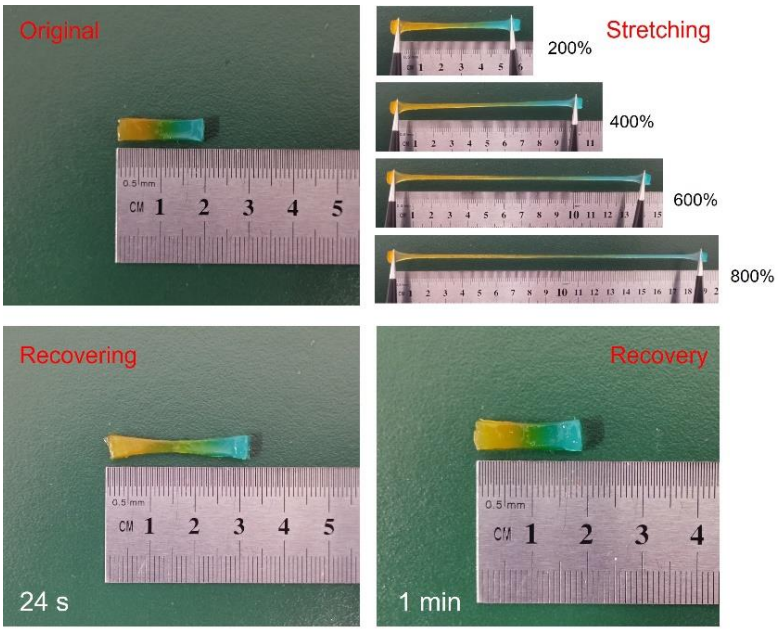

Figure S16. Optical images showing the excellent self-recovery performance of the healed hydrogel.

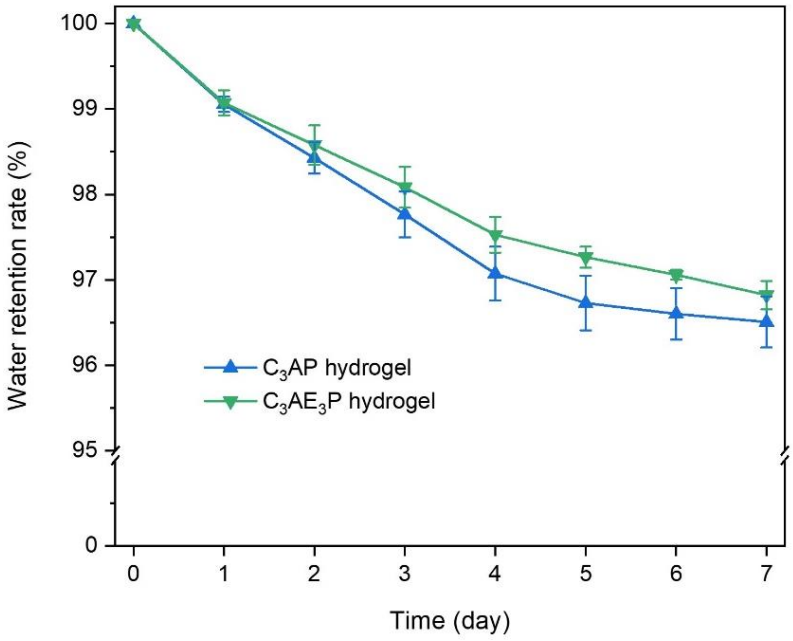

Figure S17. Water retention as a function of time when placing the hydrogel under the condition of room temperature. Error bars showing the SD with sample size of 6.

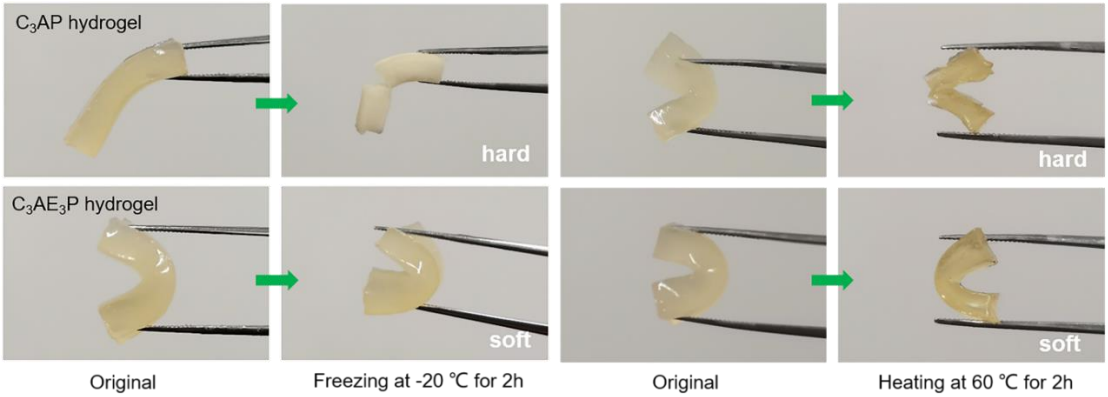

Figure S18. Display of the C_3AP and C_3AE_3P hydrogels after freezing at -20 °C or heating at 60 °C.

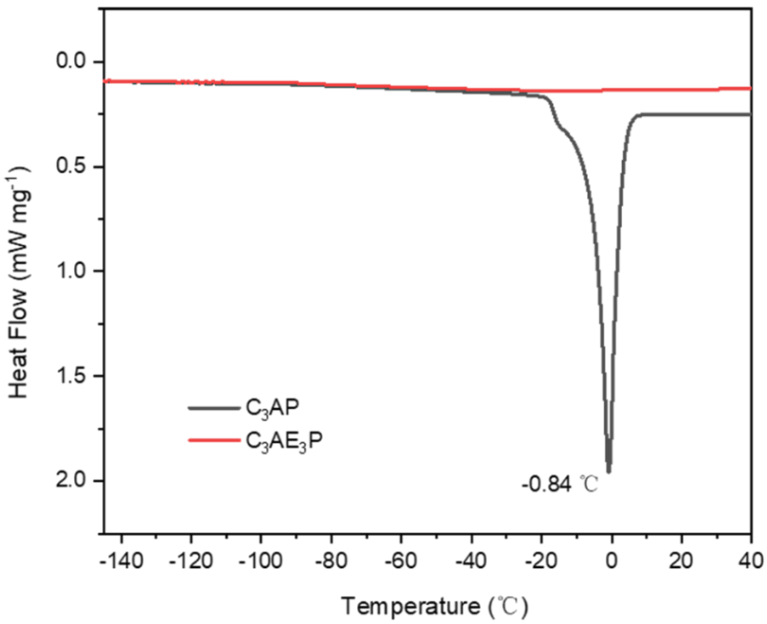

Figure S19. DSC thermograms of C_3AP and C_3AE_3P hydrogels from -145 °C. to 40 °C., the heating rate was 5 °C·min^{-1}.

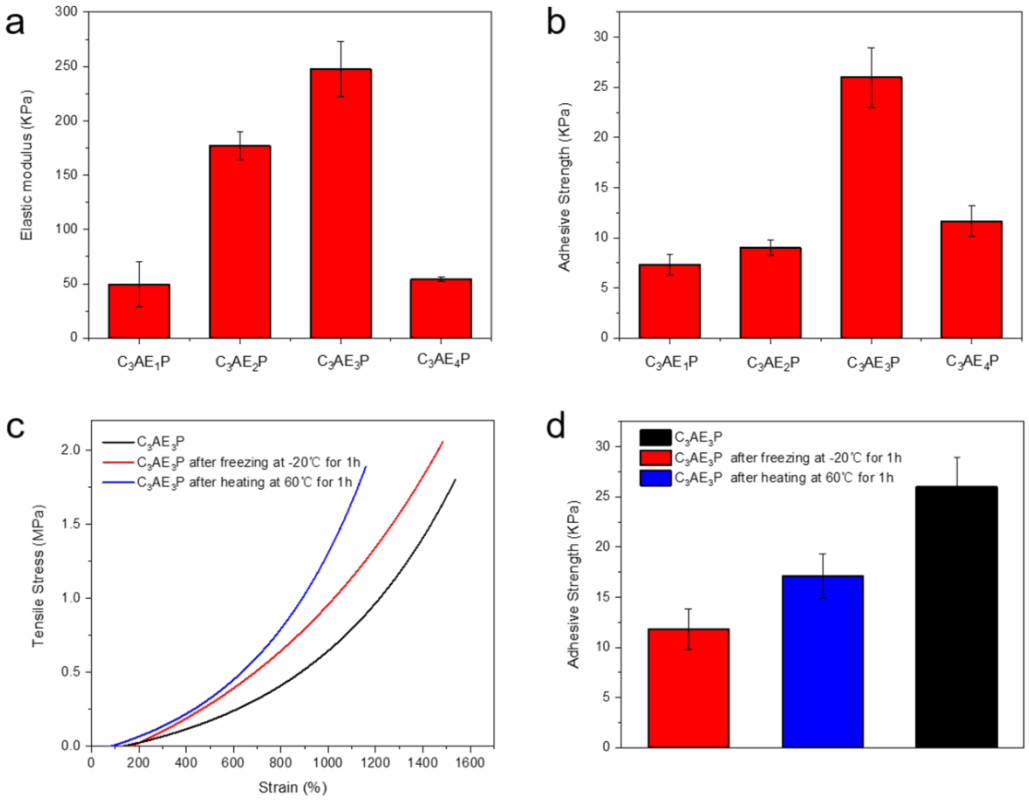

Figure S20. (a) The tangle elastic modulus was calculated from the stress-strain curves of the CAEP hydrogels. **(b)** The adhesive strength of the CAEP hydrogels. **(c)** Tensile stress-strain curves and **(d)** adhesive strength of the C_3AE_3P hydrogel under different conditions.

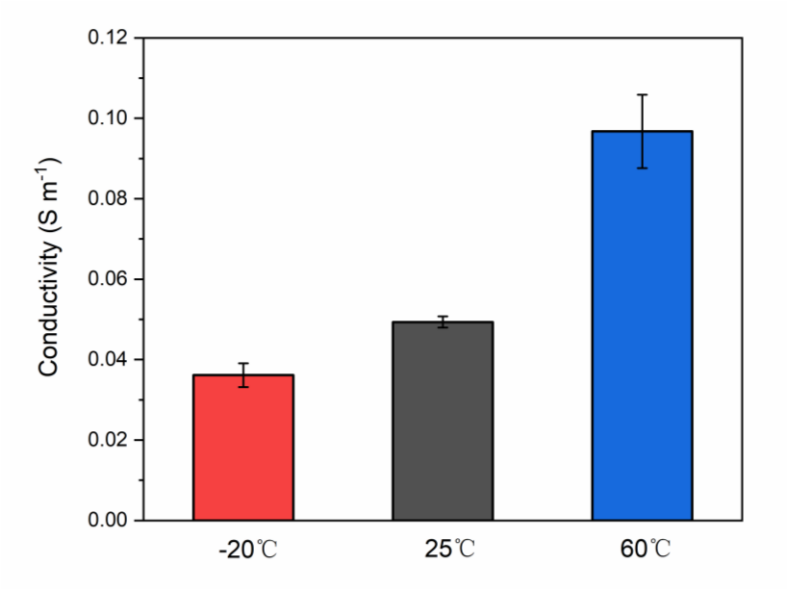

Figure S21. Electrical conductivity of C_3AE_3P hydrogel at different temperatures.

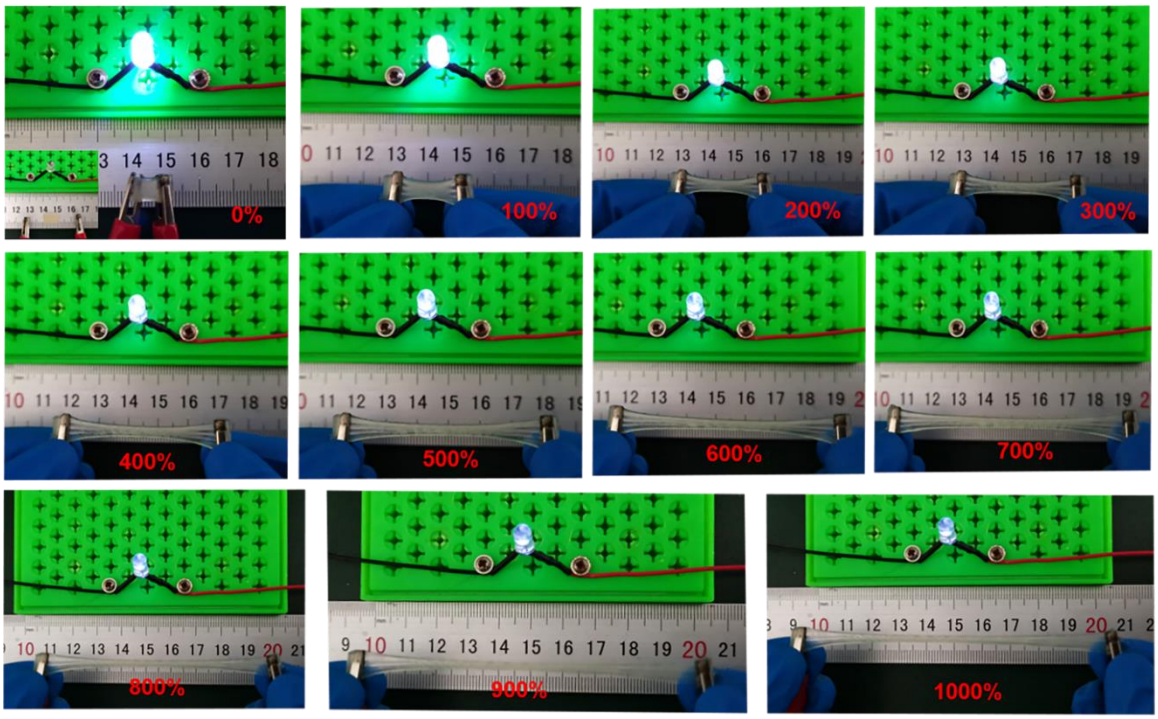

Figure S22. Optical images demonstrate that the C_3AE_3P hydrogel can be used as a conductor in circuits and the bulb became dimmed during stretching.

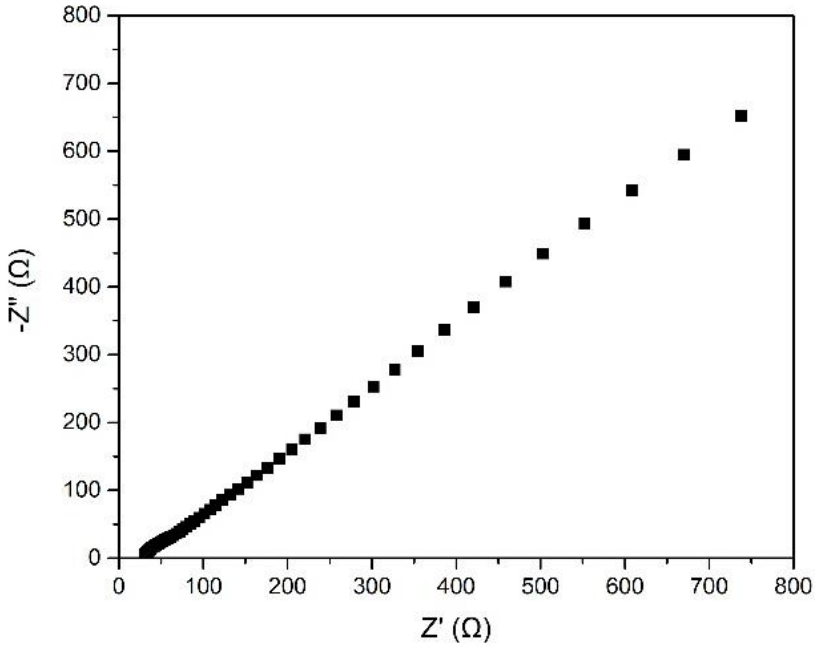

Figure S23. Electrochemical impedance spectra of the C_3AE_3P hydrogel.

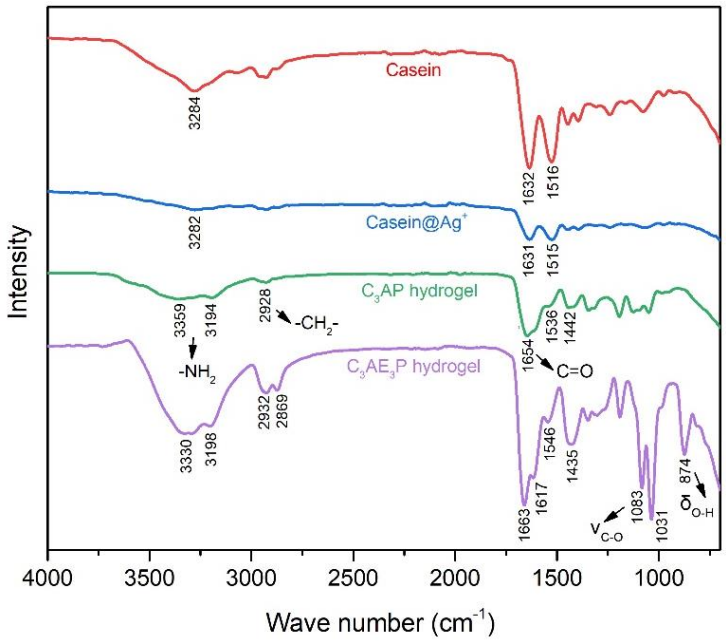

Figure S24. FT-IR spectra of Casein, Casein@Ag^+, C_3AP hydrogel and C_3AE_3P hydrogel. The primary characteristic peaks of casein at 3284, 1632, 1516 cm^{-1} were amino groups, carbonyl groups, N-H bending, and C-N stretching vibration, respectively. For C_3AP hydrogel, 3359 and 3194 cm^{-1} were absorption peaks of free and associated amino groups, respectively. 2928 and 1442 cm^{-1} were vibration peaks of methylene, and 1654 cm^{-1} was the absorption peak of carbonyl groups. For C_3AE_3P hydrogel, the characteristic peaks of EG at 1083, 1031, and 874 cm^{-1} were C-O stretching vibration and O-H bending vibration, respectively. The shifting of stretching vibration of O-H from 3359 to 3330 cm^{-1} indicates the formation of hydrogen bonding between water and EG molecules.

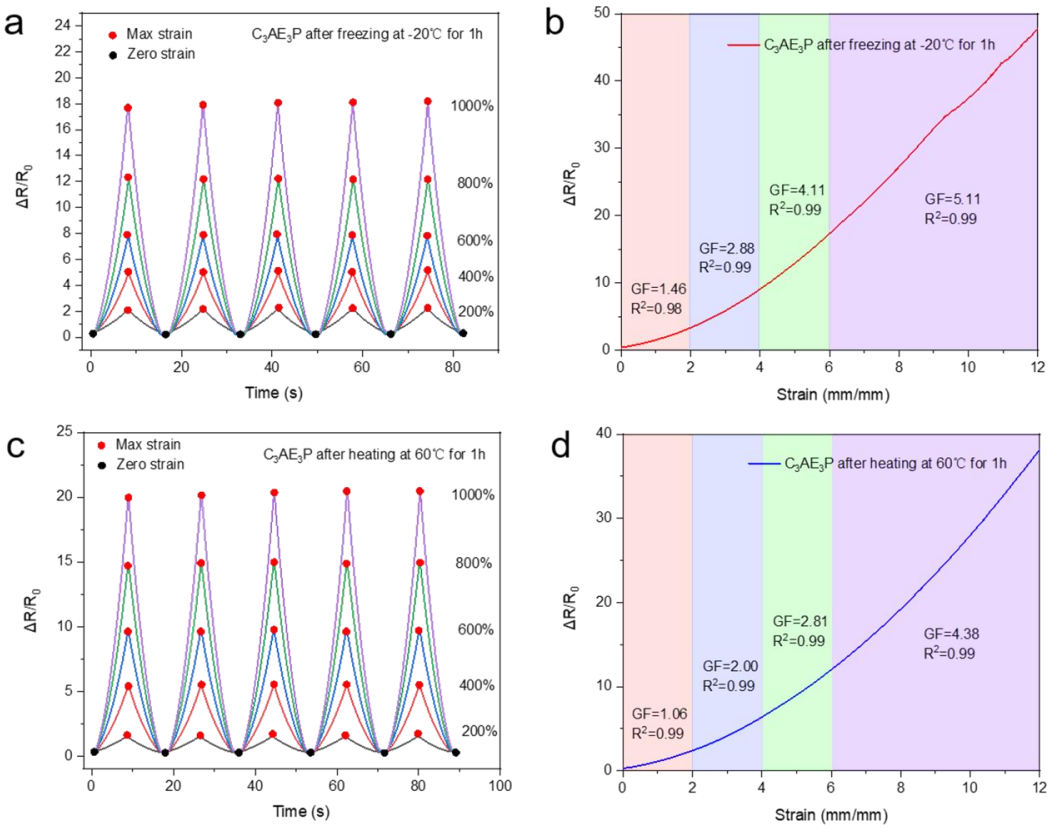

Figure S25. (a, c) Variation in the relative electrical resistance of C_3AE_3P hydrogel under different conditions during 5 stretching-releasing cycles with the fixed strains of 200, 400, 600, 800, and 1000%, respectively. **(b, d)** The tensile conductivity curves of C_3AE_3P hydrogel under different conditions.

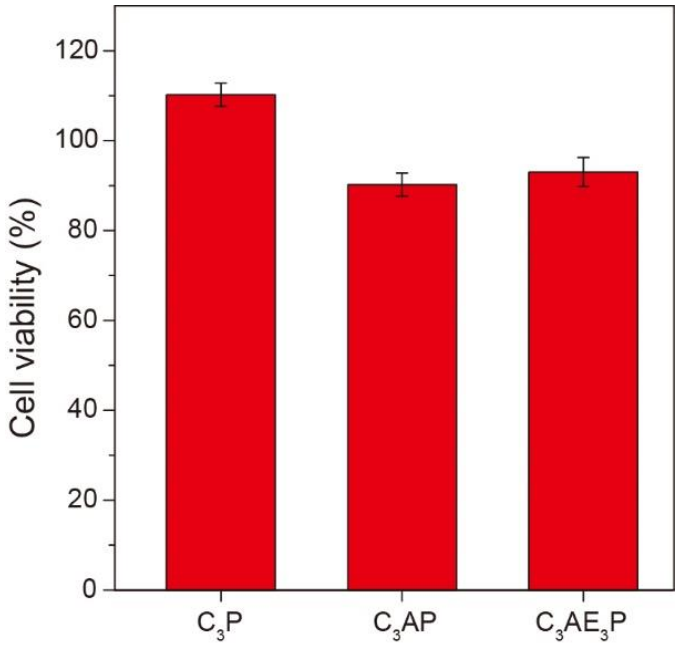

Figure S26. Cell cytotoxicity study of hydrogels. Error bars showing the SD with sample size of 6.

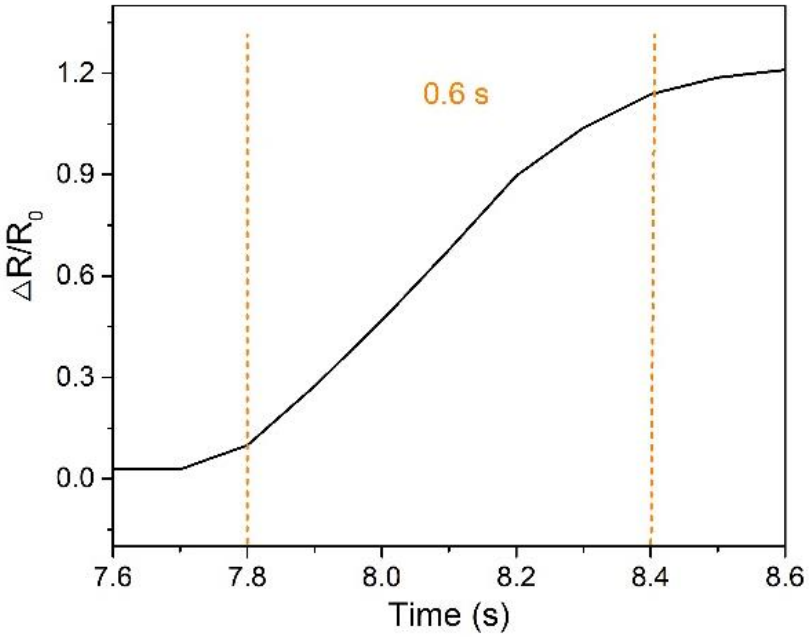

Figure S27. Response rate of the C_3AE_3P hydrogel.

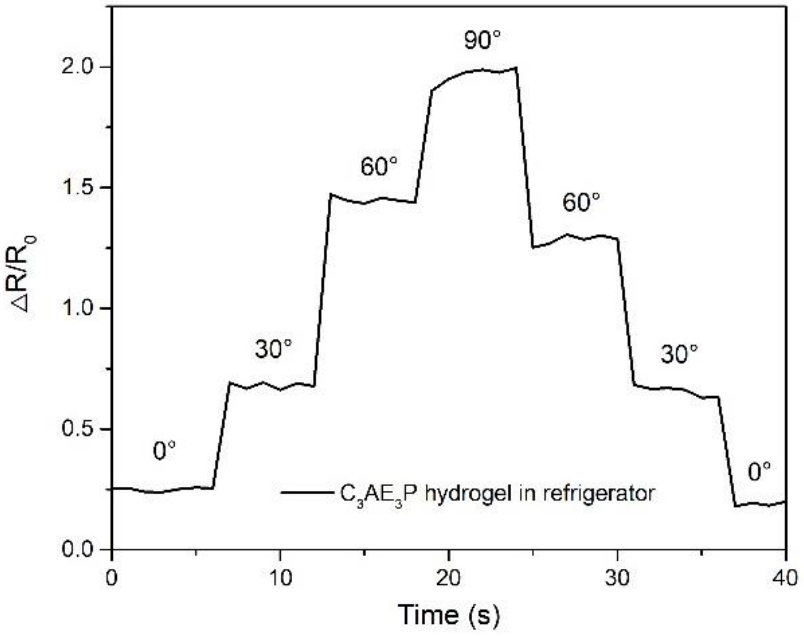

Figure S28. Sensing performance of C_3AE_3P hydrogel recorded in refrigerator at -20 ^oC.

Table S1. Contents of the various hydrogels.

Hydrogel	**Casein (wt%)**	**Ag^+ (mg)**	**V_{EG}/V_{NaOH} solution**	**BACA (mg)**	**MBA (mg)**	**AM (g)**	**Irgacure 2959 (mg)**
PAM	0	0	0	0	2.0	1.0	3.0
C_3P	15	0	0	0	2.0	1.0	3.0
C_1AP	5	0.05	0	2.0	0	1.0	3.0
C_2AP	10	0.05	0	2.0	0	1.0	3.0
C_3AP	15	0.05	0	2.0	0	1.0	3.0
C_4AP	20	0.05	0	2.0	0	1.0	3.0
C_3AE_1P	15	0.05	1/2	2.0	0	1.0	3.0
C_3AE_2P	15	0.05	1/4	2.0	0	1.0	3.0
C_3AE_3P	15	0.05	1/6	2.0	0	1.0	3.0
C_3AE_4P	15	0.05	1/8	2.0	0	1.0	3.0